IEEE Photonics Journal
An IEEE Photonics Society Publication

Open Access

Direct and Practical Identification for Back Focal Plane Based Surface Plasmon Microscopy

Volume 12, Number 1, February 2020

Bei Zhang
Qiusheng Wang
Ang Li
Xiqi Wang

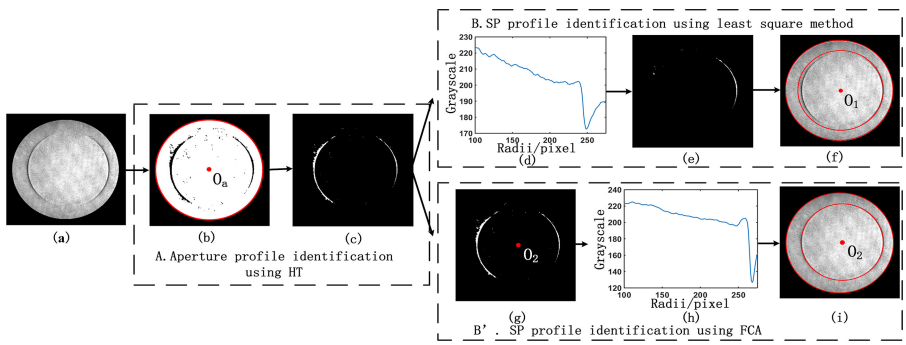

DOI: 10.1109/JPHOT.2019.2959801

Direct and Practical Identification for Back Focal Plane Based Surface Plasmon Microscopy

Bei Zhang, Qiusheng Wang, Ang Li, and Xiqi Wang

Department of Automation Science and Electrical Engineering, Beihang University, Beijing 100191, China

DOI:10.1109/JPHOT.2019.2959801

Manuscript received December 4, 2019; accepted December 9, 2019. Date of publication December 16, 2019; date of current version January 7, 2020. This work was supported by the National Natural Science Foundation of China (NSFC) under Grant 61405006 and in part by Fundamental Research Funds for Central Universities, China. Corresponding author: Bei Zhang (e-mail: bei.zhang@buaa.edu.cn).

Abstract: We propose a practical approach to identify plasmonic absorption profile on back focal plane (BFP) of surface plasmon microscopy (SPM). Compared to previous morphology approaches, the proposed one features: i) it is applicable in BFP images with non-concentricity; ii) the algorithm of Fourier Correlation Analysis (FCA) maximizes SPP while minimizes random coherent noises, which makes it extremely suited for BFP images with significant low-quality; (iii) it takes much less time for one identification process and the entire identification can be operated automatically.

Index Terms: Surface plasmon microscopy (SPM), hough transform, fourier correlation analysis (FCA), back focal plane (BFP).

1. Introduction

Surface plasmon microscopy (SPM) combines high sensitivity of Surface plasmon (SP) and spatial resolution of optical microscopy [1]. It excites SP using an immersion objective with high numerical aperture (*NA*). Intensity SPM is the most common and compact one in practice. Its basic concept is to measure SP absorption profile on the back focal plane (BFP) and is also defined as BFP-typed SPM. Previous literatures have comprehensively studied the theory, modelling and principle of SP excitation in objective-coupled SPM. However, rare studies on rapid and high-precision identification of plasmonic absorption profile have been reported. This work aims to study the identification of plasmonic absorption profile on BFP of SPM. Theoretically, properties of a tested sample can be characterized by identifying SP absorption profiles. However, in practice, SP absorption profiles are covered by severe coherent noise, especially when using coherent illumination as the light sources, which imposes great challenges on the identification and limits automatic operation of SPM instrument. Besides, low identification precision decreases the measurement precision of SPM and slow identification speed limits its applications in fast phenomenon tracing and image mapping from batches of experimentally acquired images. An obvious and simple approach is to capture the 1-D intensity data along the p-polarized radius on BFP [2], [3]. It performs well in simulated BFP or experimentally recorded BFP images with almost no noises; however, it suffers from low precision when handling BFP images of low quality. An optimized method is to capture the 1-D intensity data along the s-polarization and p-polarization respectively and obtain a relatively

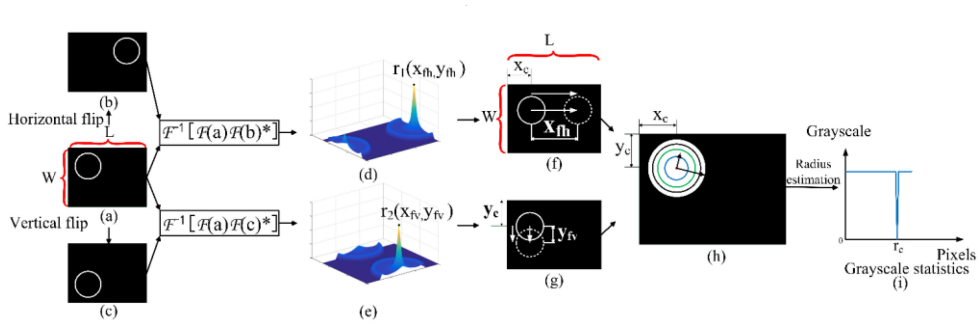

Fig. 1. Fourier correlation analysis. (a) The original image; (b)(c) The horizontally and vertically flipped images; (d)(e) Cross-correlation matrix between the original image and the flipped images; (f)(g) The horizontal and vertical translations between the original image and the flipped images according to the calculated cross-correlation matrix in (d) and (e); (h) Identification of the absorption profile center and intensity statistics of the radius; (i) Identification of the radius.

accurate plasmonic absorption profile by dividing the two sets of intensity data [4]. The latter approach, however, still uses the 1-D intensity data and is vulnerable to random noises. Since the absorption profile of SP exhibits as 2-D distribution on the BFP, it is suggested to fit with a circle [5] as it can average the effect of random noises and give a smaller standard deviation. However, it is laborious to manually fit it especially when it is applied in batch processing (imaging mode) or fast phenomenon tracking (sensing mode). It is inevitable to operate automatic identification. We previously proposed morphology [6], which worked well but with two conditions: 1) when SP absorption and aperture profiles were concentric; 2) the coherent noises were not severe. To properly overcome the mentioned difficulties, this work proposes to use Fourier Correlation Analysis (FCA) to independently identify the plasmonic absorption profile. The basic principle is that plasmonic absorption profile is symmetric and exhibits high correlation between the original BFP image and the horizontally / vertically flipped images respectively while the coherent noises are randomly distributed and give low correlation in cross correlation. The property of independent identification makes the proposed approach applicable in practical SPM instruments with slight misalignment and the characteristics of FCA greatly enhances the proposed approach in handling severe coherent noises. Moreover, it takes much less time for one identification process since no strict and complicated morphological processing and filtering are required when operating FCA. This work focuses on identification and readers are suggested to refer principles and operations of the intensity scanning SPMs in [1], [7], wide-field SPMs in [8] and interferometric SPMs in [9].

2. Principle of Fourier Correlation Analysis

Three algorithms are involved in this work: Hough transform (HT), Fourier correlation analysis (FCA) and intensity statistics. The readers are suggested to refer [6] for details on HT and intensity statistics. We utilize FCA to independently identify the center of SP absorption profile since it maximizes the symmetric SP signal and minimizes the randomly distributed coherent noise. Fig. 1(a) gives the original image with horizontal and vertical lengths of L and W respectively. Then we first flip the cropped image horizontally (Fig. 1(b)) and vertically (Fig. 1(c)). The correlation coefficient r of the cropped image f_1 and the horizontally flipped image f_2 is calculated by:

$$r = \mathrm{F}^{-1}\left[\mathrm{F}\left(f_1\right)\mathrm{F}\left(f_2\right)\right] \tag{1}$$

where $F(f_i)$ is Fourier transform of the image f_1 or f_2. By finding the maximum value of the correlation coefficient as labeled 'r_1' and 'r_2' in the correlation matrix (Fig. 1(d) (e)), we can obtain relative translation (x_{fh}, y_{fv}) between original image and horizontally / vertically flipped image as shown in Fig. 1(f) (g). According to the size of the original image, the center of the SP absorption profile

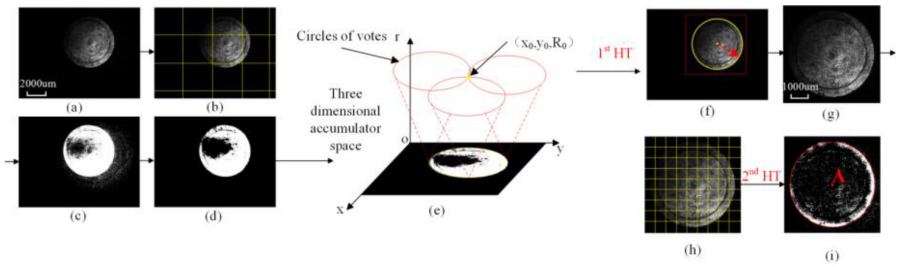

Fig. 2. Identification of aperture profile: (a) Original image; (b) blocking; (c) Binary image; (d) Image after filtering; (e) Hough transform; (f) Identified result using 1st HT; (g) The cropped image; (h) 2nd blocking; (i) Accurate identification.

(Fig. 1(h)) can be obtained by

$$\begin{cases} x_c = (L - x_{fh})/2 \\ y_c = (W - y_{fv})/2 \end{cases} \tag{2}$$

3. Procedures of Identification

This section is to introduce how to operate the identification in experimentally acquired BFP images from an intensity scanning SPM. The optical arrangement is the same as that in [6]. We use a He-Ne laser with a wavelength of 632.8 nm and an objective lens with a *NA* of 1.25. The light source is in radial polarized mode. The sensor-chip is composed of BK7 (substrate), Au film of 46 nm (coupling agent) and sputtering coated MgO thin films (tested samples). In the experiment, the thicknesses of the sputtered MgO layers are initially controlled by crystal oscillators in the magnetron sputter, which gives a precision with an error below 0.1 nm. After that, in order to obtain an independent measure of the thicknesses of the layers, they are measured from the top surface using a spectroscopic ellipsometer (alpha-SE@Woollam).

3.1 Identification of Aperture Profile Using HT

To show the effectiveness and good performance of the proposed method, we extract the SP absorption profile from experimentally acquired BFP images with extraordinary uneven brightness and poor quality (Fig. 2(a)). The original image contains large background which not only reduces the identification accuracy but also increases the calculation amount and memory space. To solve this problem, we roughly locate and crop the region of interest (ROI) in the original image. Considering the severe unevenness and low-quality, we firstly get the binary image of BFP using combination of global threshold and local threshold to enhance the contrast between aperture profile and background. The threshold is obtained using the minimum error method [10]. Fig. 2(b) shows the blocking process and Fig. 2(c) gives the binary image. Since the binary image contains severe discrete noises, the morphology techniques such as the corrosion, expansion and filtering are applied to the binary image (Fig. 2(c)) and obtain the processed image (Fig. 2(d)). Then we operate the 1st HT and acquire the center and radius of the aperture in the parameter space. Fig. 2(e) and (f) show the principle of HT and the roughly identified result respectively. The cropped image is shown in Fig. 2(g). Now we operate the 2nd HT on the cropped image to accurately identify the aperture profile. The process is similar as that of 1st HT except that a smaller block size is applied to enhance the detail information as shown in Fig. 2(h). Since the cropped image contains less background areas with extra noisy spots and the details within the aperture profile should be remained, it is not suggested to utilize the filtering processing in this stage. The accurately identified center and profile of the aperture profile are shown Fig. 2(i). The radius of the aperture profile takes

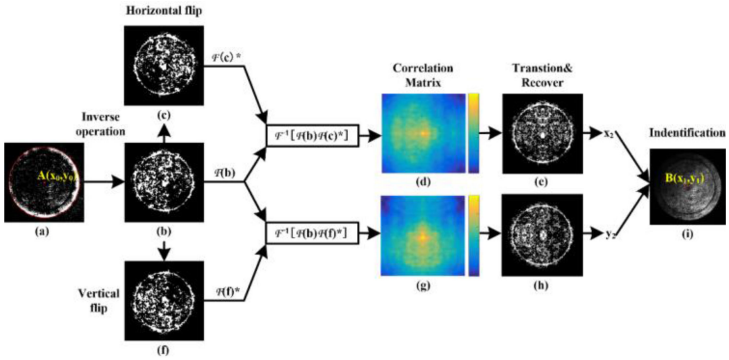

Fig. 3. Identification of SP profile using FCA. (a) The cropped image; (b) The filtered image; (c)(f) Horizontally and vertically cropped image; (d)(g) Correlation coefficient between the original image and the horizontally/vertical flipped image; (e)(h) The matched image using the calculated offset; (i) The cropped image with the identified center of the SP absorption profile.

270.6 pixels and the applied *NA* is 1.25. According to Abbe's criteria, we can get:

$$\frac{\mathrm{R}_A}{R_{SP}} = \frac{NA}{n_{oil}\sin\theta_{sp}} \tag{3}$$

where R_{A} and R_{sp} are the identified radii of outer aperture profile and inner SP absorption profile respectively, n_{oil} is the refractive index of the matching oil and θ_{sp} is the optimal SP excitation angle.

3.2 Identification of SP Absorption Profile Using FCA

Fig. 3 shows the procedures on how to independently identify the center of SP absorption profile by FCA. To eliminate the influence of aperture profile on the correlation, we need to remove the outer aperture profile to reduce its influence on identification of SP absorption profile. One effective solution is to blur the boundary. Considering that the intensity around the outer aperture profile is brighter due to the scattering of the boundary, we carry out reverse operation (Eq. 4) on the cropped image (Fig. 3(a)) to blur the boundary (Fig. 3(b)).

$$f(i,\,j) = \begin{cases} 0 & (i-x_0)^2 + (j-y_0)^2 \geq R_0 \\ f'(i,\,j) & (i-x_0)^2 + (j-y_0)^2 < R_0 \end{cases} \tag{4}$$

where $f(i,\,j)$ is the intensity value at each pixel in the image matrix after binarization; $(i,\,j)$ is the location of the pixel in the image matrix; $f'(i,\,j)$ means to reverse the pixel value. $A(x_0, y_0)$ and R_0 are the coordinate and radius of the aperture profile. We firstly flip the image in Fig. 3(b) horizontally and obtain Fig. 3(c); secondly conduct Fourier transform on the two images respectively and multiply the Fourier transform results; thirdly operate inverse Fourier transform to obtain the correlation coefficient matrix between the two images (Fig. 3(d)). The maximum value indicates the best correlation between the original image and flipped image. And the index of the maximum value in the correlation matrix is functional related with the translation of the SP absorption profile before and after the flip which gives the abscissa x_1 of the center of the SP absorption profile as expressed in Eq. 2. With the same steps, we obtain the ordinate y_1 of the SP absorption profile. The corresponding steps are shown in Fig. 3(f) (g) (h). The identified center $B(x_1, y_1)$ indicated in Fig. 3(i) does not coincide perfectly with center of the aperture profile $A(x_0, y_0)$ but gives a few pixels difference. When the sample tilts seriously, the difference of the centers become larger. This demonstrates that it is significantly important to independently identify center of the SP absorption instead of directly using that of the outer aperture profile. After that, we select the minimum value in the radial intensity statistics to determine the radius of the absorption profile since SP on BFP features on a dark region. We show the radial intensity statistics in Fig. 4(a) and (b). We calculate

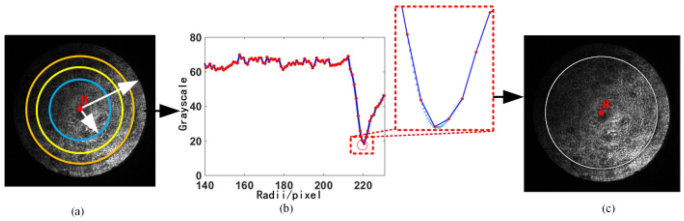

Fig. 4. (a) Intensity statistics; (b) Intensity statistics and interpolation; (c) The identified center ('B') and SP absorption profile.

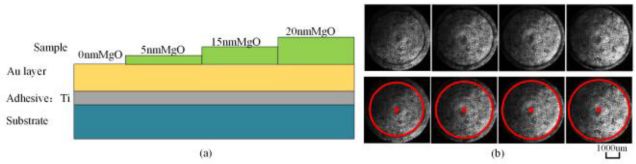

Fig. 5. Sample characterization. (a) Sample structure; (b) Experimental BFP images and the recognition results; from left to right, the thickness of MgO materials is 5 nm, 15 nm, and 20 nm respectively; (c) Measurement result of different samples.

TABLE 1
Measurement Result of Different Samples

Layer	R_{sp} (pixel)	θ_{sp}(°)	Angle error	MgO(nm)	Error
5nmMgO	233.5	44.36	0.01	5.05	1%
15nmMgO	242.1	46.46	0	15	0%
20nmMgO	248.2	48.00	0.13	20.4	2%

(c)

the average intensity of every circle centered on point 'B' along the radial direction and acquire the distribution statistic as Fig. 4(b). We also use spline interpolation (cyan dot in Fig. 4(b)) to enhance the identification accuracy. The final identification result is shown in Fig. 4(c), including the center (red spot) and SP absorption profile (white circle). The full process takes 970 ms on average to identify one SP absorption profile in the test (CPU: Core i7-4770 with 16GB memory). In practice, it is unnecessary to operate the full process since the outer aperture profile and the center of the SP absorption profile is fixed. Only the statistically calculation is required and it takes much less time (∼98 ms) which enables fast identification.

3.3 Application of the Identification in Thickness Measurement

Here we verify the precision of the identification method. Fig. 5(a) demonstrates the sample structure, in which, standard BK7 cover glass is used as the substrate with a thickness of 0.17–0.19 mm and refractive index of 1.518. All the nano-layers are deposited by magnetron sputtering, including 46 nm of Au layer and 1 nm of Ti layer. The MgO layer is coated on top of the Au layer with a thickness of 5 nm, 15 nm, 20 nm respectively. Experimentally acquired BFP images are given in the first row of Fig. 5(b). One can see apparently that the SP absorption profile radii increase with the thickness of MgO layers. We process the captured images with the proposed identification approach and acquire the radii of SP circles as shown in the second row of Fig. 5(b). Fig. 5(c) shows the measurement result of different samples. As identified in Section 3.1, the radius R of the aperture profile is 270.6 pixels. Considering the *NA* of 1.25, the identified radii of the three samples are 233.5, 242.1 and 248.2 (pixels), which correspond to SP excitation angles of 44.36°, 46.46° and 48° respectively. Table 1 gives the measurement results. The experimental results demonstrate

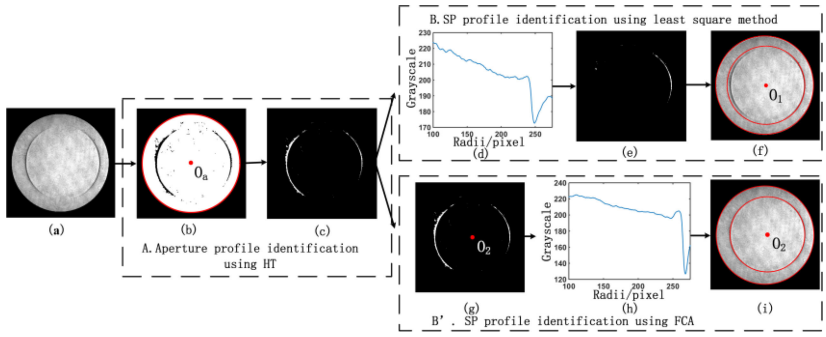

Fig. 6. Comparison of the FCA approach and Morphology [6]. (a) BFP images with obvious non-concentricity; Stage A: The common procedure: (b) Aperture identification using HT; (c) The processed SP profiles. Stage B: Morphologic identification. SP identification using 'common' center and least square method. (d) Grayscale statistics; (e) Remaining SP profile using the roughly identified SP radius; (f) The identified SP profile. Stage B': The FCA approach. (g) The independently identified center of SP profile using FCA; (h) Grayscale statistics using the identified center in (g); (i) Identified SP absorption profile using FCA.

excitation angle errors of 0.05°, 0° and 0.2° respectively. By the Fresnel multilayer equations [4], we can obtain the thickness of the MgO nano samples of 5.05 nm, 15 nm and 20.4 nm. The actual thickness errors are 0.05 nm, 0 nm and 0.4 nm. The coated error is below 1 nm. It shows that the identification method gives accurate results in nano-material measurement and indicates efficiency of the approach.

4. Discussion

4.1 Comparison Between FCA and Morphology in Non-Concentric BFP Images

The proposed approach allows independent identification of SP and thus allows accurate identification for practical systems with severe non-concentricity in experimentally acquired BFP images caused by system aberration or tilt samples. Fig. 6 shows the comparison of the two approaches in identifying non-concentric BFP images. For better comparison of the two approaches, we use an experimental BFP image with severe non-concentricity (Fig. 6(a)). Stage *A* shows the common procedures for the two approaches. Fig. 6(b) shows the identified aperture profile using HT and Fig. 6(c) gives the SP profiles after removing the outer aperture profile. Stage B and B' show the SP absorption profile identification using Morphology and the presented FCA respectively. The former one is to employ the identified center 'O_a' in Stage A as the center of SP 'O_1' and then operate the grayscale statistics along the radius to find the minimum (Fig. 6(d)), which gives the SP profile. It is obvious that the SP absorption profile is improperly located since part of SP absorption profile is removed (Fig. 6(e)) due to the severe non-concentricity and gives inaccurate identification results (Fig. 6(f)). Instead, the presented approach utilizes FCA to accurately identify the center of SP profile ('O_2' in Fig. 6(g)) and then identify the exact SP absorption profile by operating the intensity statistics along the radius (Fig. 6(h)). The result in (Fig. 6(i)) shows clearly that the presented FCA can effectively and properly identify the SP absorption profile.

4.2 Comparison Between FCA and Previous Morphology in Noises

This section is to prove that the proposed FCA enables suppression of coherent noises and gives higher accuracy compared with morphology. For better comparison, we assume that all the images possess perfect concentricity. We operate Monte-Carlo by adding random noises to noise-free BFP images and repeat n times ($n = 500$). We add Gaussian noise with mean value as 0 and variance as 0.01 to generate 500 BFP images. Then we apply the two approaches to identify the

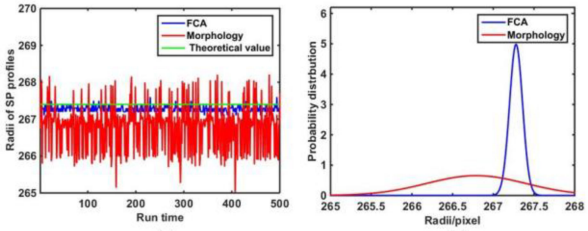

Noise(var)		0.01	0.015	0.02
Morphology	Mean	266.79	266.51	266.54
	Std	0.61	0.64	0.64
FCA	Mean	267.28	267.29	267.32
	Std	0.080	0.088	0.14

(c)

Fig. 7. (a) SP absorption profile radius distributions using morphology and FCA respectively. (b) The corresponding probability distributions of the two approaches. (c) The identified results of the two approaches with different noise levels.

SP absorption profiles. The red and blue curves in Fig. 7(a) show the identified result curves when using Morphology and FCA respectively. The results show clearly that the present FCA method gives much smaller derivation and more stable results than morphology. Besides, its mean value is much closer to the theoretical value. Fig. 7(b) gives the probability distributions curves of the two methods to better illustrate the comparison and Fig. 7(c) shows the identified results of the two approaches with different noise levels. It is obvious that the present FCA method gives relatively accurate results close to the standard value with great probability, which proves that the present algorithm can effectively reduce impact of the coherent noises. It is not because of the added one more step of FCA but the characteristics of the proposed approach. Firstly, although both of the two methods apply the algorithm of HT, the accuracies of the identifications are different. For the proposed method, the identification of inner SPR profile is determined by the FCA, which shows insensitivity to coherent noises and can still give high-precision of identification for the case of severe noise levels. However, for morphology, the identification accuracy is totally determined by the identified center by HT. For the case of relatively severe noises, HT takes account of the noises as effective elements and thus gives lower accuracy. Secondly, the present method identifies the SP absorption profile by operating the intensity statistics on the original grayscale BFP image and thus can accurately locate the optimal SP profile within a dip band with a certain width. However, the morphology is to locate the SP absorption profile using the binary image and thus the pixels within the SP dip with a certain width are taken into account in the identification of SP absorption profile, which further decreases the identification accuracy.

5. Conclusion

We presented a direct and practical approach to identify plasmonic absorption profiles in BFP-based SPM. It featured on three aspects: 1) it allowed independent identification of aperture and plasmonic and thus was applicable in practical SPM instruments with concentric BFP images due to slight misalignment; 2) it could handle experimentally acquired BFP images with relatively severe coherent noises thanks to the characteristics of the proposed FCA algorithm; 3) compared to previous morphologic approaches, it required rare manual operation and the entire procedures were operated automatically. Detailed comparisons between the proposed approach and previous morphologic method were given. It could be directly applied in various BFP involved SPMs.

References

[1] H. Kano, "Excitation of surface plasmon polaritons by a focused laser beam," *Near-Field Opt. Surface Plasmon Polaritons*, vol. 81, pp. 189–206, 2001.
[2] J. Zhang, M. C. Pitter, S. Liu, C. See, and M. G. Somekh, "Surface-plasmon microscopy with a two-piece solid immersion lens: bright and dark fields," *Appl. Opt.*, vol. 45, pp. 7977–7986, 2006.
[3] H.-M. Tan, "High resolution angle-scanning widefield surface plasmon resonance imaging and its application to bio-molecular interactions," Ph.D. thesis, Dept. Elect. Electron. Eng., Univ. Nottingham, Nottingham, U.K., 2011.

[4] A. W. Peterson, M. W. Halter, A. L. Plant, and J. T. Elliott, "Surface plasmon resonance microscopy: Achieving a quantitative optical response. Review of Scientific Instruments," *Rev. Sci. Instrum.*, vol. 87, 2016, Art. no. 093703.
[5] R. Wang *et al.*, "Plasmonic petal-shaped beam for microscopic phase-sensitive SPR biosensor with ultrahigh sensitivity," *Opt. Lett.*, vol. 38, pp. 4770–4773, 2013.
[6] B. Zhang, C. Zhang, Q. Wang, P. Yan, and J. Wang, "Identification of plasmonic absorption profile in surface plasmon microscopy using morphology," *IEEE Photon. J.*, vol. 10, no. 6, Dec. 2018, Art. no. 4501809.
[7] K. J. Moh, X.-C. Yuan, J. Bu, S. W. Zhu, and B. Z. Gao, "Surface plasmon resonance imaging of cell-substrate contacts with radially polarized beams," *Opt. Express*, vol. 16, pp. 20734–20741, 2008.
[8] B. Huang, F. Yu, and R. N. Zare, "Surface plasmon resonance imaging using a high numerical aperture microscope objective," *Analytical Chem.*, vol. 79, pp. 2979–2983, 2007.
[9] B. Zhang, C. Zhang, M. G. Somekh, P. Yan, and L. Wang, "Common-path surface plasmon interferometer with radial polarization," *Opt. Lett.*, vol. 43, pp. 3245–3248, 2018.
[10] M. S. Sayed, "Robust fabric defect detection algorithm using entropy filtering and minimum error thresholding," in *Proc. IEEE 59th Int. Midwest Symp. Circuits Syst.*, 2016, pp. 365–368.